Electric-field Induced Criticality and Frequency Responsive Dynamics of Charged Rods

Kyongok Kang[*1] and J. K. G. Dhont*[1]

[1] Forschungszentrum Juelich, ICS-3 (Soft Condensed Matter), Juelich, 52425, Germany

ABSTRACT

We use the suspensions of charged fibrous virus (fd) as a model system for charged colloidal rods, where thick electric double layers are present. In particular, the system has shown the electric-field induced phase/ state transitions under a low electric field strength. We briefly present the frequency responsive dynamics in the phase/state diagram and field-induced criticality in the dynamical states, by approaching the field-induced critical point. In addition, the possible mechanism of low-frequency responsive dynamical states is briefly explained by the local charge redistribution of dissociation and association of condensed ions on the charged rods. The found phases/states are unique in the bulk phase diagram, away from the electrode polarization that is dominant near to the surface of the ITO glasses, in the sense that they are observed independent from the applied field amplitude and frequency.

KEYWORDS

Electric double layers, Electric phase/state diagram, image-time correlation, field-induced criticality, local charge dissociation/ association, frequency responsive dynamics, charged fibrous virus (fd) suspensions, multiphase-transitions, polarization, hydrodynamic interactions

I. INTRODUCTION: System and Electric Phase/ State Diagram

The experiments discussed here are performed with suspensions of charged chiral fd-virus particles, which consist of a DNA strand covered with about 2700 fd-coat proteins, carrying approximately 10,000 elementary charges [1, 2]. The length of a fd-virus is 880 nm, and the bare diameter is 6.8 nm, with a persistence length of approximately 3 μm. A number of liquid crystalline phases have been observed in these systems at a relatively high ionic strength,

larger than 1 mM [3-5], and the electric-field induced birefringence at low fd-concentration have been reported (up to about 6 times larger than the overlap concentration) at very low ionic strengths, of 0.01 mM [6]. There are no studies reported yet on the phase behavior at low ionic strength, in the range of 0.01 - 0.5 mM, where electrostatic interactions are dominant and packing effects lead to the formation of a glass. The system of charged fd-viruses is chosen as a model system for charged colloidal rods. Some of the important features of suspensions of fd-virus particles are as follows: First, the fd-virus particles, cultured from the E-coli bacteria, are long and thin, stiff, mono-disperse DNA strands, as determined by transmission electron micrograph (TEM) morphology [1]. Second, the surface of virus is covered by fd-coat proteins in a helical fashion that carries many elementary charges. Third, since these charged rods are highly anisotropic, they develop orientational order when the concentration is increased. Here the suspension is prepared at a low ionic strength, where the Debye screening length is about 3 times larger than the bare diameter of fd-rods, and the aspect ratio change sufficiently the phase behaviors. Particularly where there is isotropic and nematic phase coexistence, within the so-called "biphasic" region, the electric response of these charged rods are explored. Now when the external electric field is applied, the various phases/states are induced, shown in the electric-field induced non-equilibrium phase/state diagram in Figure 1, as in the applied field amplitude versus frequency diagram, together with the corresponding depolarized morphologies of each of the phases and states. The electric response of unique phases and states are shown in Figure 1, depicted with depolarized morphology as local orientational order: At high frequencies, large than about 1 kHz, a uniform homeotropic H-phase is found where the rods are aligned along the electric field. Below 1 kHz, however, on increasing the field strength, first a chiral nematic phase is formed (denoted as N*), and on further increasing the field strength a dynamical state is formed (the D-state), where nematic domains melt and form [7-14]. The interest here is in the dynamics of melting and forming of small nematic domains in the D-state, as well as the particle dynamics in the H-phase. The depolarized optical morphologies are shown under an in-situ electric field cell, shown in Figure 2, where the in-situ cell is located under a depolarized optical microscope, while the AC sinusoidal waveform is applied through the cell gap of 1.4 mm. The bright region is the charged fd-rods are more or less aligned as compare to the black background in an isotropic phase, shown in the morphology of the N-phase. As one can see in the Figure 1, there is threshold field amplitude for both low- and high- frequency responses, entering the chiral-nematic phase (N*) and homeotropic-phase (H), respectively. We will discuss further the different interactions of many interacting charged rods these two difference phases under an applied electric field.

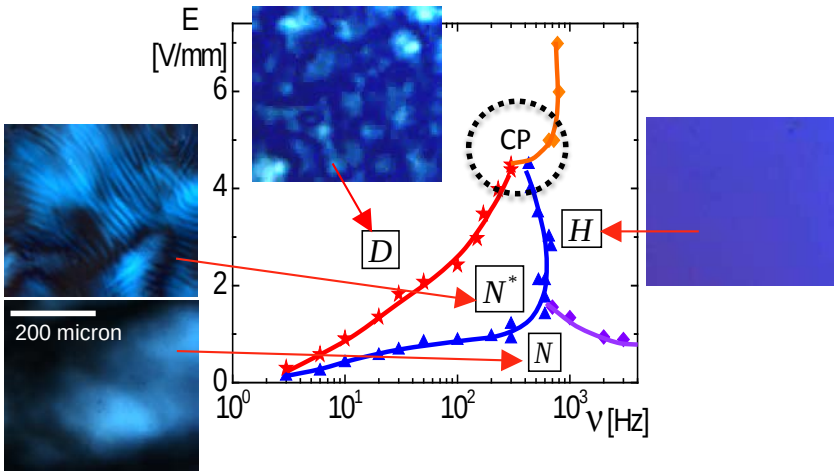

Figure 1: An electric phase/ state diagram of charged fibrous viruses (fd) in the AC field amplitude and frequency: In the absence of field, nematic-domains in the isotropic background (N-phase), chiral-nematic phase (N*), dynamical state (D) and homeotropic phase (H). Multiphases meet at the critical point (CP) at a critical frequency and amplitude. Two sharp phase transitions (blue and red lines) are induced at below the critical frequency, while as one transition line is observed at higher frequency.

II. Image Time-Correlation Functions in Dynamical States

For the dynamics of orientation textures that is the characteristic of low-frequency induced dynamical states, the melting/ forming of small nematic domains are quantified by the construction of image-time correlation functions [15, 16]. The principle of image-time correlation is briefly sketched in Fig. 3. First, a series of time-lapsed images is collected with a CCD camera. Note that the pixel averaged intensity is subtracted from the single pixel intensity, and the function is normalized such that it is unity at time zero. Then the decay rate of correlation functions is used to characterize the slowly varying dynamics of textures. For a data acquisition, the time binning (or time interval), the total number of frames and the region of interest are optimized. From time-lapsed images are collected to represent the dynamical events of textures, reconstructed by a series of black/ white bitmap formats. Here, the pixel sizes are chosen as 170 by 170 pixels, which can be slightly varied with an optimization between total numbers of image frames and time binning. Each time frame image intensity values are stored in an Ascii format to calculate pixel-to-pixel correlations at different time frames, normalized to an initial time frame.

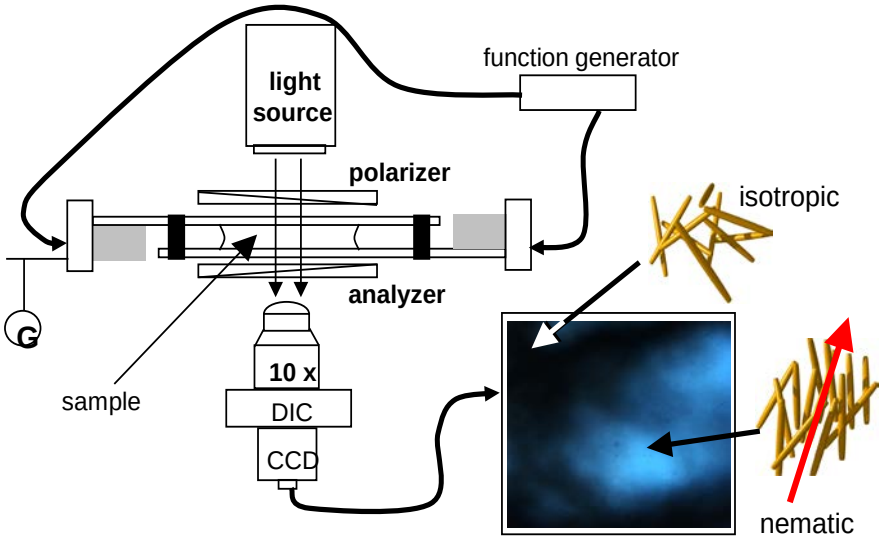

Figure 2: Schematic of the equipment for an in-situ electric field optical cell for depolarized microscopy. In the absence of an external field, the system has isotropic (black background) and nematic (blue domain) phase is coexistent. For the broader region of view, 10X objective lens is used under microscope. The field of view of the morphology is about 400 x 400 μm^2 .

Then the enhanced images are appeared as black and white bitmap format. From these images, image time-correlation functions are constructed, which are defined as,

$$C_V(t) = \frac{\left\langle \left[I(t) - \langle I(t) \rangle \right] \left[I(0) - \langle I(0) \rangle \right] \right\rangle}{\left\langle \left[I(0) - \langle I(0) \rangle \right]^2 \right\rangle}, \qquad (1)$$

where $I(t)$ is the intensity of a pixel at time t , while the brackets $\langle \cdots \rangle$ indicate averaging over all pixels. Figure 3(a) has shown a simple sketch of field-induced phase/state diagram with spatial-temporal images for a slow-dynamical state (Ds) and a fast dynamical state (D_f), respectively. The corresponding time-lapsed images are shown on the left panel of Figure 3(a). The performance of an image-time correlation function is shown in Figure 3(b), on the dynamical states in low-frequencies electric field, where the slow dynamical state becomes faster as the field amplitude is increased. This can be fitted with a single stretched exponent, and the characteristic time τ is the measure for melting and forming of small nematic domains in the field-induced dynamical states. We have found

the criterion for time binning is at least 3-10 times faster than the dynamical events to get reasonable background and statistics in the correlation functions. Typically 1s, and 0.3s are used for slow, and fast dynamical states, respectively.

III. Electric-field Induced Criticality in Dynamical States

The top left plot in Figure 4(a) shows the characteristic time of small nematic domains (size of 30-400 μm), as obtained from the image-time correlation functions, either on approaching the "non-equilibrium critical point", so-called CP in Figure 4(c) that is indicted within the red dashed circle, by increasing the frequency (see the left blue horizontal line in the phase/state diagram). There is a power-law divergence of the time scale τ on which melting and forming of nematic domains proceeds, as the critical point is approached. Also the size of domains diverges, as shown in the left plot below, and a logarithmic divergence is found (see the most right of Fig. 4(b)). A stronger divergence of both the length and time scale is observed at the critical frequency, by lowering the field amplitude, on approaching the "non-equilibrium critical point" [11-13]. There is also an evidence of critical slowing down particle dynamics on the approach of the critical point from the side of the H-phase, as it can be seen from the dynamic light

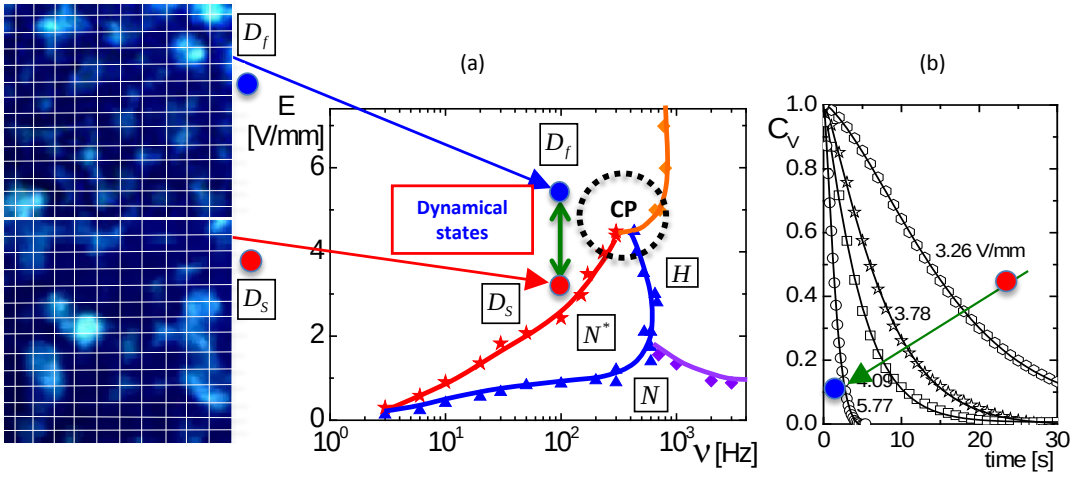

Figure 3: (a) Spatial-temporal images for dynamical states: for slow-dynamical states (Ds) versus fast dynamical states (D_f), and the field-induced phase state/ diagram. (b) Example of an image-time correlation function as an increase of field amplitude. The regions of interest (ROI's) are indicated as squares.

scattering correlation functions of a high-frequency response, on the right-side of phase/state diagram. There, clearly a non-vanishing slow mode appears in earlier time, on approach of the critical point, and sustains for long waiting time [11]. Non-equilibrium criticality for characterizing the time of melting and forming of small nematic domains, the image-time correlation functions are used that we just introduced in the previous chapter. To extract the critical slowing down of observables, one should take care of non-critical background contributions that is ambient as a steady state, as indicated by the red arrows on the left in Figure 4(a) and (b). The critical parameter can be determined by looking for the divergence of the "observables", in other words, the inverse of the "observables" (in this case the time and domain size) becomes zero, which is depicted in the middle, as blue arrows in Figure 4(a) and (b). The external parameters can be then either the applied frequency or the field amplitude. The most right panels has shown both "strong", as a power-law like, or "weak", as logarithmically, as a function of the frequency. Figure 4(c) shows the summary of divergences of field-induced critical exponents of time and domain-size divergence, for approaching the critical points by different pathways in the phase/state diagram. Much stronger divergence is found at the critical point at a fixed frequency by lowering the field amplitude. Also the critical slowing down behaviors is observed for the microscopic particle dynamics, at the high frequency side, where a uniform homeotropic phase is formed [10]. On the contrary, by reducing the frequency, and field amplitude below the critical point, systematic changes of the DLS correlation functions are observed [11, 12]. However, at the critical field amplitude, the slow mode is dominant for both far away from the transition line, and closer to the critical point, which is apparent with much long time thermal fluctuations in the scattered amplitude.

IV. Local Charge Dissociation/Association of Condensed Ions in Dynamical States

A possible mechanism of limiting cycle of melting and forming of small nematic domains in the field –induced dynamical states is discussed [17], and presented with the local charge dissociation/association of condensed ions that is depicted in Figure 5: (I) When the external field is applied at a low ionic strength, thick electric double layers are present surrounding of the charged fd-virus core, shown in the most right bottom in Figure 5. Local charge dissociation of condensed ions occur to release of condensed ions to the bulk solution, perpendicular to the rods, allowing transiently an increase of ionic strength. (II) At a relatively higher ionic strength in bulk solution induces the double layers of charged fd-rods become thinner. Consequently, it contributes to an effective diameter thinner

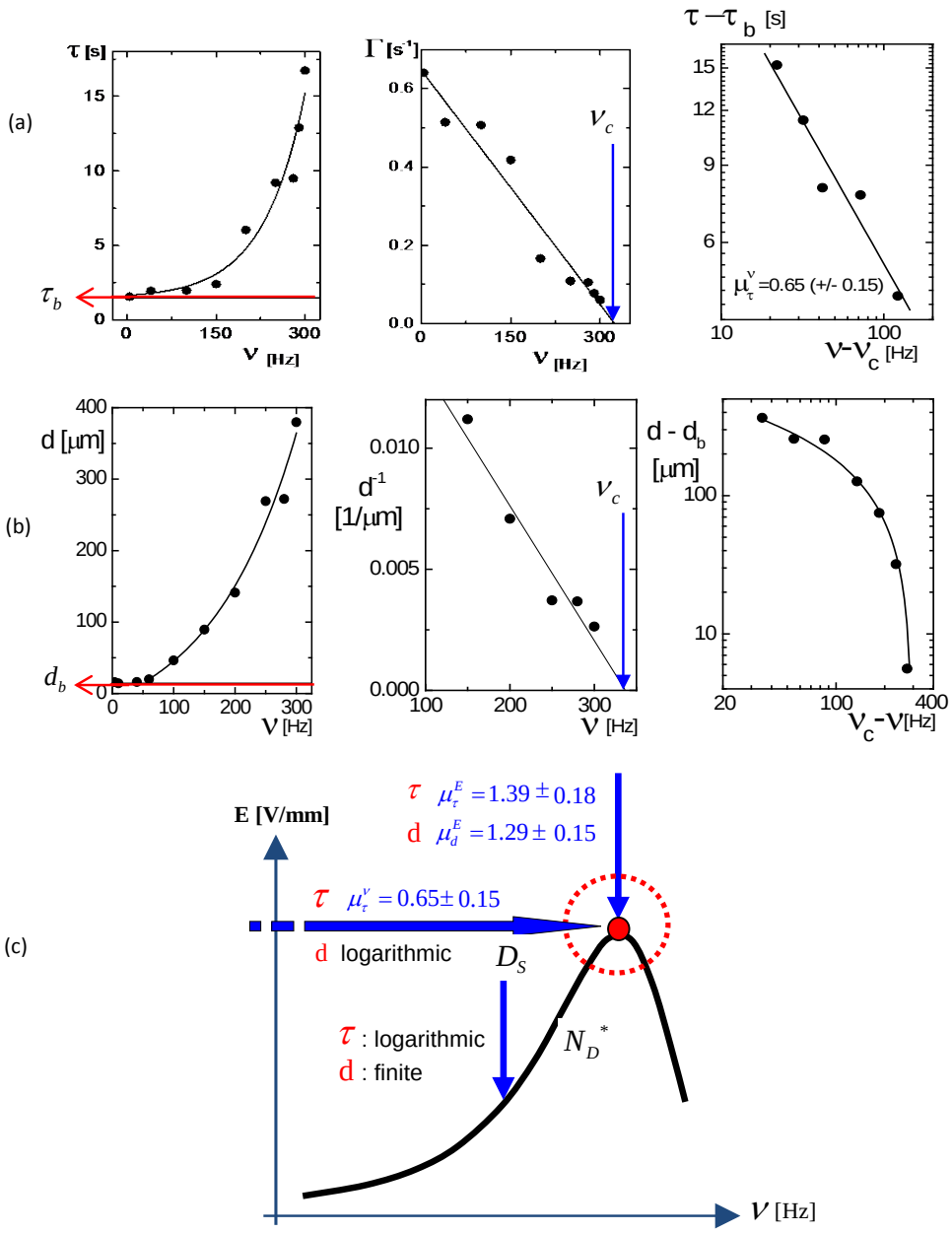

Figure 4: (a) Decay times and (b) domain size as a function of applied frequency, and (c) a summary of the divergences of decay times and domain sizes of melting and forming of small nematic domains in the dynamical states. The divergence power is indicated in different pathways in the phase/states diagram amplitude and frequency plane, by approaching the critical point.

via time dependent electric double layers, $d_{eff}(\kappa^{-1}(t))$. Thus it is easy to align but still unstable state, shown in the most right top in Figure 5. (III) The system decays instantaneously towards isotropic states, where the association of condensed ions takes place. (IV) Local charge association of condensed ions perpendicular to the rods allow the de-aligned states as meta-stable state with a relatively thicker effective diameter, and (V) the orientation order increase via rotational motion of the charged fd-rods under an external field amplitude to recycle the limit of dynamical states (I). The semi-quantitative theory of the limit cycles of field-induced dynamical states with some fitting parameters are discussed in ref. [17].

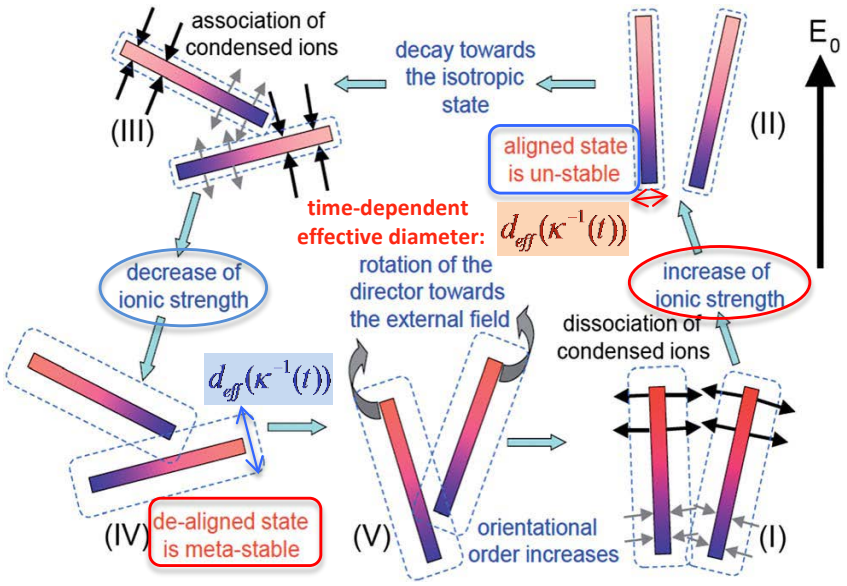

Figure 5: A proposed mechanism of low-frequency-induced dynamics states, where the limit cycle of melting and forming of small nematic domains are observed in the slow/ fast dynamical states, in an oscillating field.

V. Unique Frequency Responsive Dynamics: Polarization versus Hydrodynamics

Finally, unique distinguishable dynamics of frequency responses are shown in Figure 6, as the electric field-induced phase/state diagram. The low frequency-responsive dynamics are dominated by the electrostatic interactions via induced polarization; where mobile ions are accessed in the thick electric double layers (see the left side of Figure 6). However for higher frequency-responsive dynamics, polarization is not important, but the hydrodynamic interactions become important via electro-osmotic flow in solvent (on the right side of Figure 6).

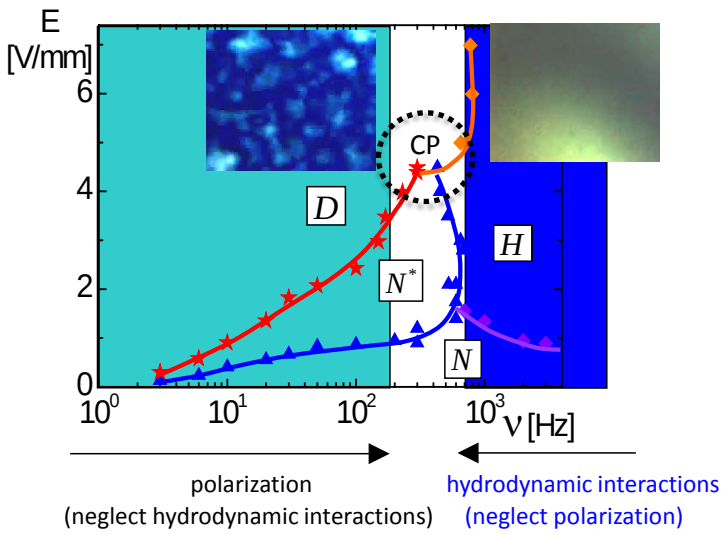

Figure 6: A simpler electric field-induced phase/state diagram, where two different interactions regimes are distinguished as either low- or high-frequency responsive dynamics. In between, there is a critical slowing down regime where the field-induced multi-critical phases meet.

VI. Conclusion

Demonstrated field-induced criticality is characterized by an image-time correlation spectroscopy in the low-frequency dynamical states, Ds - D_f state transition, by approaching the multicritical point. Also by reducing the frequency, near to the H-N* transition line, high-frequency responsive dynamics is exhibited by the critical slowing down behaviors. The system has shown rich and unique field-induced phase-transitions in the sense that they are independent from the way the field is applied. Therefore, it can be introduced as truly an intelligent system for the electric responses of many interacting charged rods.

Acknowledgment

This research received no specific grant from any funding agency in the public, commercial, or not-for-profit sectors.

REFERENCES

1. Levy, J.A., Heinz, F-C., and Owens, R.A. (1994). *Virology*, 3rd edition, Prentice Hall, NJ.

2. Zimmermann, K., Hagedorn, J., Heuck, C.C., Hinrichsen, M., and Ludwig, J. (1986). The ionic properties of the filamentous bacteriophages pf1 and fd., J. Biol. Chem, 261(4): 1653-5.

3. Fraden, S. (1995). *Phase transitions in colloidal suspensions of virus particles, in observation, prediction and simulation of phase transitions in complex fluids*, ed. Baus, M., Rull, L.F., Ryckaert, J.P., Kluer Academic Pub., Dorefrecht, 460, NATO-ASI-series.

4. Dogic, Z., Fraden, S. (2000). Cholesteric phase in virus suspensions. Langmuir. 16: 7820-7824.

5. Dogic, Z., Fraden, S. (2001). Development of model colloidal liquid crystals and the kinetics of the isotropic-smectic transition. Philos. Trans. R. Soc. A., 359: 997 -1015.

6. Kramer, H., Graf, C., Hagenbuechle, M., Johner, C., Martin, C., Schwind, P., and Weber, R. (1994). Electro-optic effects of aqueous fd-virus suspensions at very low ionic strength. J. Phys. II, France 4: 1061 – 1074.

7. Kang, K., Wilk, A., Patkowski, A., and Dhont, J.K.G. (2007). Diffusion of spheres in isotropic and nematic networks of rods: Electrostatic interactions and hydrodynamic screening. J. Chem. Phys. 126: 214501-1 -17.

8. Kang, K., Dhont, J.K.G. (2008). Double-layer polarization induced transitions in suspensions of colloidal rods. Eur. Phys. Lett. 84: 14005-p1 –p6.

9. Kang, K., Dhont, J.K.G. (2010). Electric-field induced transitions in suspensions of charged colloidal rods. Soft Matter. 6: 273-286.

10. Kang, K., Dhont, J.K.G. (2009). Criticality in a non-equilibrium, driven system: Charged colloidal rods (fd-viruses) in electric fields. Eur. Phys. J. E. 30: 333-340.

11. Kang, K. (2010). Charged fibrous viruses (fd) in external electric fields: dynamics and orientational order. New. J. Phys. 12: 063017.

12. Kang, K. (2010). Diffusivity in an electric field-induced homeotropic phase of charged colloidal rods. Eur. Phys. Lett. 92: 18002-p1 –p5.

13. Dhont, J.K.G., Kang, K. (2010). Electric field –induced polarization and interactions of uncharged colloids in salt solutions. Eur. Phys. J. E. 33: 51-68.

14. Dhont, J.K.G., Kang, K. (2011). Electric field-induced polarization of the layer of condensed ions on cylindrical colloids. Eur. Phys. J. E. 34: 40.

15. Kang, K. (2010). Mesoscopic relaxation time of dynamic image correlation spectroscopy. J. Bio. Sci. Eng. 3: 625-632.

16. Kang, K. (2011). Image time-correlation, dynamic light scattering, and birefringence for the study of the response of anisometric colloids to external fields. Rev. Sci. Instrum. 82: 053903-1 -9.

17. Dhont, J.K.G., Kang, K. (2014). An electric-field induced dynamical state in dispersions of charged colloidal rods. Soft Matter, 10, 1987-2007.